

Microstructure and mechanical properties of new die-cast quaternary Al-Cu-Si-Mg alloys

Qing Cai, Chamini L. Mendis, Isaac T.H. Chang*, Zhongyun Fan

Brunel Centre for Advanced Solidification Technology (BCAST), Brunel University London, Uxbridge UB8 3PH, United Kingdom

*Corresponding author: isaac.chang@brunel.ac.uk

Abstract

Three new ultrafine hypoeutectic die-cast alloys based on quaternary Al-Cu-Si-Mg system were developed. The CALPHAD thermodynamic modelling of Al-Cu-Si-Mg system based on Scheil description was conducted to predict the volume fractions of the eutectic mixtures. The designed volume fraction of eutectic mixtures of Al-xCu-2.2Si-1.1Mg ($x=5, 6.6$ and 10.6 wt%) alloys were determined to be 0.2, 0.25 and 0.3, respectively. With the increase in eutectic fraction, the yield strength and ultimate tensile strength increased from 219 MPa to 267 MPa, and 344.7 MPa to 395 MPa respectively, while the elongation to fracture decreases from 7.72% to 3.4%. The microstructure of the alloys mainly consists of Si, Al₂Cu, α -Al and Al₄Cu₂Mg₈Si₇ (Q) phases. The Al₅Cu_{2.2}Si_{1.1}Mg and Al_{6.6}Cu_{2.2}Si_{1.1}Mg alloys had similar microstructures that consisted of coarse binary/ternary and fine quaternary eutectic regions, surrounding α -Al matrix. The Al_{10.6}Cu_{2.2}Si_{1.1}Mg alloy contained α -Al grains and almost only one type of eutectic structure. The orientation relationships among Al₂Cu, α -Al and Q phases were found in the eutectic region. Al₂Cu and α -Al has a coherent interface, while the interfaces between Q and Al₂Cu as well as Q and α -Al, were found to be semi-coherent. Our results broaden a new approach to the design of die-cast alloys with multi-phase and multi-component microstructure for high-performance applications.

Keywords

Die-cast; Quaternary eutectic; Aluminium alloys; Orientation relationship

1. Introduction

The replacement of steel with light-weight materials in transport and aerospace is a promising means of improving fuel efficiency and reducing CO₂ emissions. The increased use of aluminium alloys in automobiles provides significant opportunities for weight reduction, which has real scope towards achieving emission reduction targets imposed by various environmental authorities globally. High pressure die-casting (HPDC) of aluminium components have gained much attention in recent decades, and it has been utilised in many fields, including aerospace and automotive sectors. HPDC exhibits many advantages: (a) capable of fabrication of large, thin wall and complex products; (b) high productivity; (c) good dimensional accuracy and surface finish; (d) fine microstructure and excellent mechanical properties [1,2]. In recent years, die-cast aluminium alloys have been greatly used in the automotive industry to replace heavier counterparts [3]. However, commercial aluminium alloys are not able to provide a yield strength above 200 MPa and ultimate tensile strength over 330 MPa, as well as a satisfactory ductility in the as-cast state. Thus, the development of high strength aluminium alloys becomes crucial to broaden the applications of die-cast aluminium alloys.

In recent decades, nano-/ultrafine eutectic alloys (grain size: typically between 100 to 500 nm) fabricated with high cooling rates have been highlighted in the literature, due to their exceptionally high strength [4–6]. However, binary ultrafine eutectic alloys with lamellar or fibrous microstructure exhibit poor ductility and fracture toughness at room temperature [7–9]. It is due to the high volume fraction of lamellar hard phases hindering dislocation and leading highly localised shear bands before the fracture [10,11]. For that reason, additional elements were introduced into these alloys to improve its ductility, and recently, many investigations have been carried out in ternary or multi-component of Al-, Ti-, Fe-based eutectic systems [12]. For example, in Al-based system, Park et al. fabricated ternary Al₈₁Cu₁₃Si₆ alloys using suction casting with bimodal structure, yielding a very high compressive ultimate fracture strength and plastic strain of 1.1±0.1 GPa and 11±2% respectively [13]. The ternary Al-Cu-Ni alloy containing Al₇Cu₄Ni intermetallics embedded in refined binary (α-Al and Al₂Cu) matrix was investigated by Tiwary et al [14]. The compressive fracture strength and plastic strain to failure of Al₈₈Cu_{10.5}Ni_{1.5} alloy are around 1±0.1 GPa and 9±0.1% respectively. In addition, Kim et al. studied the microstructure and compressive mechanical properties of quaternary Al₈₁Ni_{13-x}Cu_xSi₆ (x=0,3,5,8 and 10 at%) alloys [15]. The good compressive fracture strength and plastic strain were achieved in Al₈₁Ni₅Cu₈Si₆ alloy, which are 773±11 MPa and 14.8±0.7 %, respectively, owing to its multi-phase composite microstructure and fine eutectic matrix. The unique microstructure having heterogeneous

distributions of constituents with different length scale and multi-phase can usually be found in these multi-component eutectic alloys, which is named structural heterogeneity alloys [16–18]. The heterogeneous structure is favourable for the compressive ductility, while the high strength of these alloys results from the high volume fraction of strengthening multi-phases and refined eutectic structure [12,15,17,19]. The refined microstructure is based on the concept that in a multi-component alloy system, different atomic species reduce the solidification temperature of the melt, resulting in a significant increase in the constitutional undercooling. Therefore, nanoscale or ultrafine scale microstructures can be achieved.

Although these multi-component eutectic alloys have excellent compressive ductility and/or high strength [16,18,20], there is still a lack of data of its tensile properties. It is believed that the tensile ductility of these alloys is relatively low. In order to further enhance its tensile/compressive ductility, the multi-component alloys were designed to include soft primary dendrites, which is able to create more mobile dislocations during deformation [7,21–23]. These hypoeutectic alloys exhibit a combination of high ductility and desirable strength. These alloys are mainly strengthened by solute solution primary phases and refined multi-component eutectic structure.

Based on author's knowledge, there is only a little literature reporting the hypoeutectic multi-component alloys in Al-based system. Recently, Kaygısız et al. reported that the microstructure of quaternary Al-28Cu-6Si-2.2Mg (wt%) eutectic alloy consisted of α -Al, Al₂Cu, irregular Si and Q-phase (Al₅Cu₂Mg₈Si₇) and the average micro-hardness was ~200 HV [24]. This hardness value exceeds those in binary and ternary Al-based eutectic alloys such as Al-Si [25], Al-Si-Mg [26], Al-Si-Ni [27], Al-Ni-Fe [28].

The present study aims at understanding the relationship between the microstructure and tensile mechanical properties of hypoeutectic Al-Cu-Si-Mg quaternary alloys produced by HPDC process. The introduction of α -Al dendrites in hypoeutectic alloy is to balance the strength and ductility. Each hypoeutectic alloy composition is designed with a given volume fraction of quaternary eutectic mixture using CALPHAD modelling of Al-Cu-Si-Mg system. Although the Al-Cu alloys have some disadvantages such as economic costs, corrosion resistance and poor hot-tearing resistance [29–31], the approach of designing the alloys based on multi-component eutectic structures broadens the scope and introduces a new horizon for the development of aluminium alloys under rapid solidification.

2. Experimental procedure

Commercially pure Al, Fe, Cu and Mg, as well as master alloys of Al-50wt%Si and Al-20wt%Mn, were used to prepare the alloys. 6 Kg of the alloy without pure Mg was prepared in a clay crucible, which was heated in an electric resistance furnace to 780 °C. After holding the melt at a temperature of 780 °C for 3 hours, the temperature of the furnace was set to 710 °C. Once the temperature of the melt dropped to 710 °C, pure Mg (with an extra 5% in weight melt loss due to high vapour pressure of Mg) was carefully added to the melt. After 30 min holding, the melt was degassed with argon gas, with a commercial rotatory degasser at 500 rpm for 7 min. The top of the melt was covered with granular flux. After further holding for 15 min, the melt was poured into a mushroom steel mould with a bottom diameter of 60 mm for the composition analysis. The casting was ground with SiC paper from 320 to 1200. The average composition of the alloy was measured with optical mass spectroscopy (OMS). The measured compositions of the alloys are shown in Table 1.

The melt was manually dosed and released into the short sleeve of a 4500 kN HPDC machine. Standard tensile test samples of sizes similar to previous work [5], were made after each injection. The pouring temperature was set at 680 °C, which was measured with a K-type thermocouple. The tensile test mould was preheated to 250 °C for 2 hours before casting. All tensile test samples were left at room temperature for at least 24 hours before tensile testing. The Instron 5500 Universal mechanical Testing Systems equipped with Bluehill software was used for the tensile testing of the alloys. Tensile tests were conducted at room temperature. The gauge length of the extensometer and the extension rate are 50 mm and 1 mm/min, respectively.

Table 1 The measured compositions of the Al-Cu-Si-Mg die-cast alloys

Alloy Name	Solid fraction of eutectic mixture	Alloy composition (wt.%)					
		Al	Cu	Si	Mg	Mn	Fe
Al5Cu	~0.2	Balance	4.90	2.43	1.13	0.45	0.16
Al6.6Cu	~0.25	Balance	6.73	2.35	1.14	0.44	0.14
Al10.6Cu	~0.3	Balance	10.75	2.32	1.15	0.48	0.15

The microstructural characterisation was performed on a cross-section taken from the central region of the gauge length of the tensile test samples. After cold mounting, grinding and polishing, the samples were etched for 2 seconds

with 0.5% HF acid for optical microscopy (OM) and scanning electron microscopy (SEM). A Zeiss optical microscope with an attached camera and a Zeiss SUPRA 35 scanning electron microscope equipped with EDX spectrometer were used for microstructural characterisation. The volume fractions of the eutectic mixture were obtained from SEM images taken from the centre to the edge of the specimen using ImageJ software. The hardness measurements were performed using a FM-800 Vickers hardness tester using at least 5 fields for each sample with a 5 kg load and 10 s dwell time. The electron backscatter diffraction (EBSD) with a step size of 0.4 μm was used for grain size measurement. The EBSD samples were prepared via vibratory polishing with a frequency of 80 Hz for 4 h. The X-ray diffraction (XRD) samples were prepared from the vertical section of the tensile test bar near the centre of the gauge section. A Bruker D8 Advance X-ray diffractometer with Cu X-Ray radiation and Ni filter operated at a 40 kV and a 40 mA was used for phase identification. A Zeiss Auriga cross beam 420 SEM-FIB (focused ion beam) was used for the preparation of transmission electron microscopy (TEM) samples. The samples were milled to a thickness of about 80 nm attached on the Mo grid. A JEOL 2100F TEM was used to study the ultrafine microstructure of the sample. The melting and cooling curves of these alloys were determined with a Netzsch 404F1 differential scanning calorimeter (DSC) operated at a heating/cooling rate of 5 K/min and a dynamic flow of 50 ml/min of Ar gas. The 3D morphology of ultrafine eutectic was obtained via FIB-SEM tomography slices, which are provided as a video in the supplementary material. The 50% mixed backscattered and secondary electron mode was used to get the most information from each image.

3. Results

3.1 CALPHAD of the quaternary Al-Cu-Si-Mg system

The quaternary Al-Cu-Si-Mg phase diagram was reported by Mondolfo [32]. One of the quaternary eutectic points, with a composition of Al28wt%Cu6wt%Si2.2wt%Mg was selected with an equilibrium melting point of 507 °C. The CALculation of Phase Diagram (CALPHAD) modelling was used to design the current alloys based on the eutectic composition above. Fig.1 shows the simulated solidification paths of quaternary Al-Cu-Si-Mg hypoeutectic alloys with 20%, 25% and 30% eutectic mixture based on Scheil solidification modelling. The predicted compositions of these alloys with various volume fraction of eutectic mixture are shown in Table 2, and these three alloys were named Al5Cu, Al6.6Cu and Al10.6Cu, respectively. There are only three reactions in Al10.6Cu alloy, which are Liquid $\rightarrow\alpha\text{-Al}$, Liquid $\rightarrow\alpha\text{-Al}+\text{Si}+\text{Al}_2\text{Cu}$, and

final Liquid $\rightarrow\alpha$ -Al+Si+Al₂Cu+Al₅Cu₂Mg₈Si₆(Q) at 510.6 °C. In terms of Al5Cu and Al6.6Cu alloys, the binary and ternary eutectic reactions were observed (Liquid $\rightarrow\alpha$ -Al+Si and Liquid $\rightarrow\alpha$ -Al+Si+Al₅Cu₂Mg₈Si₇), following the reaction Liquid $\rightarrow\alpha$ -Al. All three alloys have the same final quaternary reaction at 510.6 °C. Due to die soldering during HPDC process and the formation of needle-like β -Al₅FeSi, minor amounts of Mn (0.5 wt%) and Fe (0.1 wt%) were added into these alloys [33,34]. The measured compositions of these three alloys are shown in Table 1.

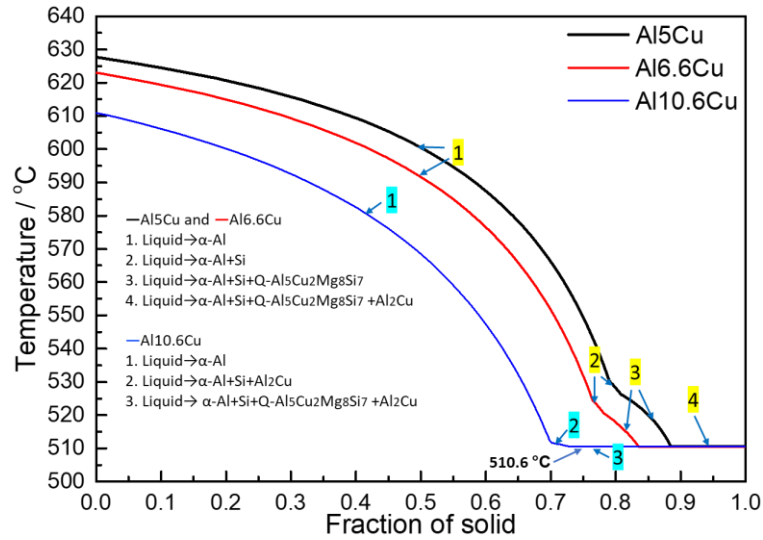


Fig.1 Simulated solidification path of die-cast quaternary Al-Cu-Si-Mg alloys predicted by Pandat 8.5

Table 2 The predicted compositions of Al-Cu-Si-Mg alloys

Alloy Name	Alloy Compositions (wt%)			
	Al	Cu	Mg	Si
Al5Cu	Balance	5	1.1	2.2
Al6.6Cu	Balance	6.6	1.1	2.2
Al10.6Cu	Balance	10.6	1.1	2.2

3.2 Microstructure

Fig.2. (a) shows XRD spectra of these three alloys which corresponded to the equilibrium phases predicted by thermodynamic calculations. Apart from eutectic phases (α -Al, Si, Al₂Cu and Al₅Cu₂Mg₈Si₆), α -AlFeMnSi phase was found, due to the addition of Mn and Fe. The heating curves of these three alloys obtained by DSC are shown in Fig.2 (b). From the heating curves in Fig.2

(b), there are only two endothermic peaks in Al10.6Cu, which coincides with the melting of the quaternary eutectic mixture and primary α -Al phase. Another endothermic peaks appear in Al5Cu and Al6.6Cu following the quaternary eutectic melting peak. From the prediction in Fig.1, these peaks correspond to the melting of binary or ternary eutectic mixture. The temperatures at which the quaternary eutectic mixture melts for the three alloys are quite similar, at $\sim 508^\circ\text{C}$, as shown in the magnified inserted image in Fig.2 (b). The alloy is fully liquid at a temperature of Al10.6Cu is 620°C , and in Al5Cu and Al6.6Cu, they are 629°C and 636°C , respectively. The experimentally determined eutectic temperatures, as well as the fully liquid temperatures, show a trend similar to that observed for the Scheil simulation result in Fig.1.

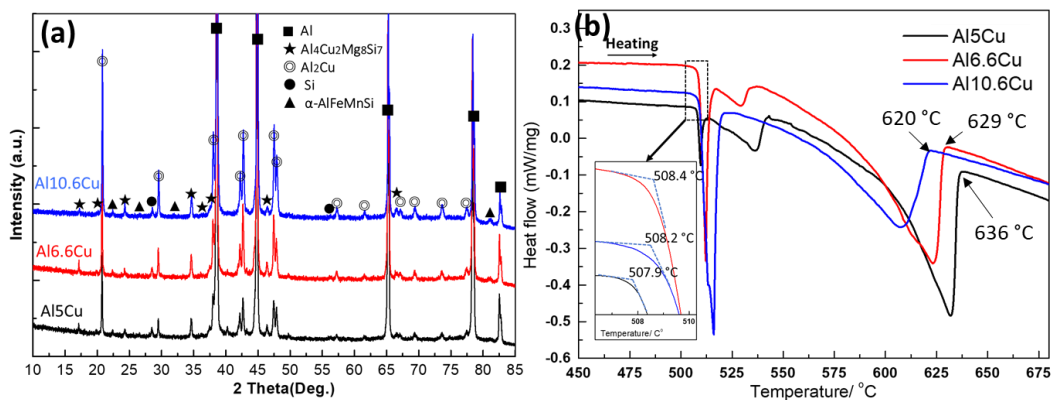


Fig.2 (a) XRD spectra (b) DSC heating curves of the die-cast hypoeutectic Al-Cu-Si-Mg alloys with a heating rate of 5 K/min

Fig.3.(a) shows a typical microstructure of Al5Cu alloy. There are two types of α -Al grains labelled α 1-Al and α 2-Al. The α 1-Al grains are coarser and solidified in the shot sleeve, while finer α 2-Al grains form in the die cavity with a much higher cooling rate [35]. Apart from Al_2Cu intermetallics at grain boundaries, there are three types of eutectic structure in Al5Cu alloy, as shown in Fig.3.(a), which are called 'EU1', 'EU2' and 'EU3' regions. The microstructures of these three eutectic regions are shown in Fig.3 (b,c,d) at high magnification. From SEM images, the eutectic structure (labelled as 'Eu1') consisted of α -Al and Al_2Cu with a lamellar spacing of 200-400 nm. The second coarse eutectic structure (labelled as 'Eu2') consisted of a lamellar spacing of 250-400 nm, as shown in Fig. 3.(c), and the grey phase was identified to be $\text{Al}_5\text{Cu}_2\text{Mg}_8\text{Si}_7$ (Q) phase. Fig.3.(d) shows the finest eutectic structure (labelled as 'Eu3') compared with 'Eu1' and 'Eu2', indicating final quaternary eutectic reaction. The microstructure of Al6.6Cu alloy is similar to that of Al5Cu alloy and is shown in the Supplementary Material (Fig.S1).

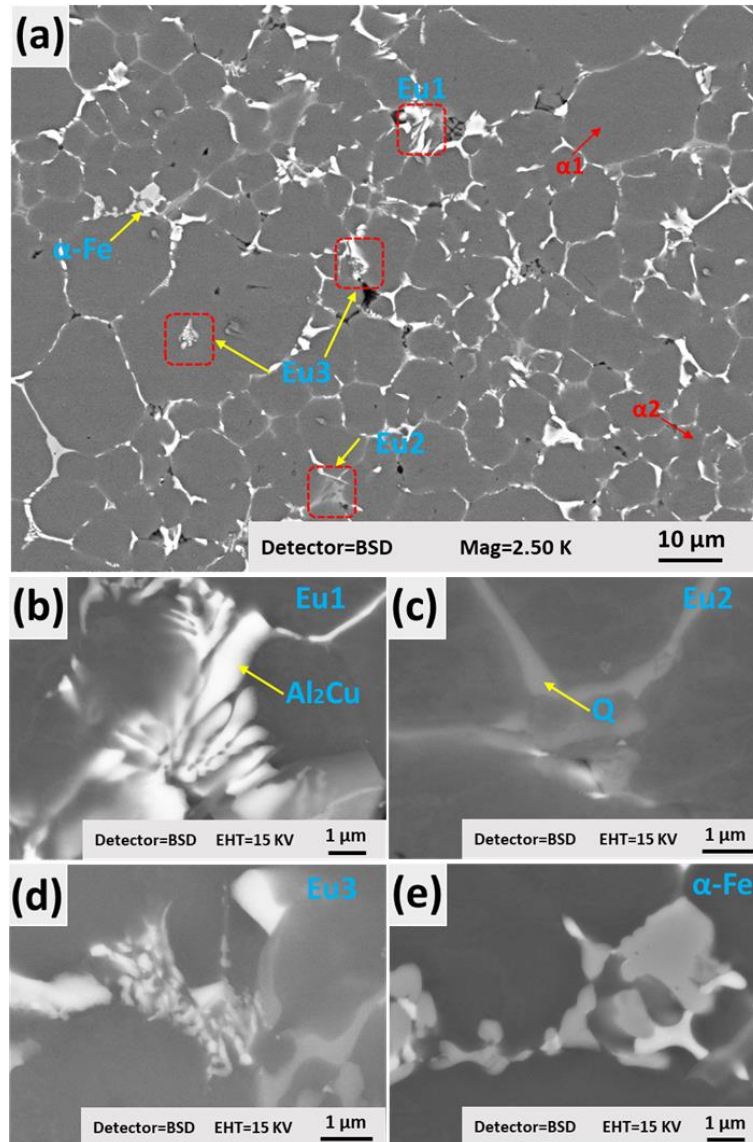


Fig.3 SEM Backscattered images showing (a) typical microstructure of Al₅Cu taken at low magnification (b) the microstructure of 'EU1', (c) 'EU2' and (d) 'EU3' (e) the fine compact α -AlFeMnSi intermetallics taken at high magnification

Fig.4 (a) shows a typical microstructure of Al_{10.6}Cu. The eutectic structure was more uniform and comprised of two different sizes of α -Al grains, together with an ultrafine eutectic structure. The magnified image in Fig.4.(b) shows the structure of such fine eutectic microstructure. The lamellar eutectic structure of α -Al-Al₂Cu was observed with an interlamellar spacing of 150-300 nm. The α -AlFeMnSi particles were observed at the boundary between the eutectic mixture and α -Al dendrites. Further characterisation with TEM of the ultrafine eutectic regions in Al_{10.6}Cu and Al₅Cu alloys will be discussed below.

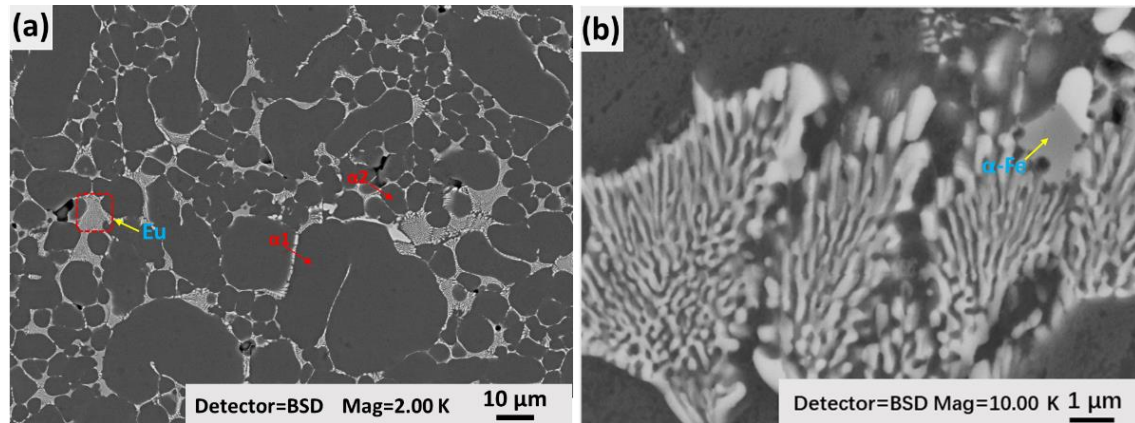


Fig.4 SEM Backscattered micrographs showing (a) typical microstructure of Al10.6Cu (b) the morphology of finer eutectic mixture

The grain structure of α -Al in these three alloys was obtained from EBSD analysis. Fig.4 (a-c) shows the EBSD grain-orientation in Al5Cu, Al6.6Cu and Al10.6Cu alloys. The corresponding statistical analysis of grain size distribution and average grain size are shown in Fig.4 (d). The bimodal size distributions of α_1 -Al and α_2 -Al grain are shown in the EBSD images. The α -Al grains show an equiaxed structure without a preferred orientation. Al10.6Cu has the finest α_1 and α_2 grains with an average size of 33.0 μm and 9.8 μm , respectively. The average grain sizes of α_1 and α_2 in Al6.6Cu are slightly finer than that of Al5Cu, which are 10.8 μm and 35.7 μm , respectively. Al5Cu alloy has the largest sizes of α_1 (38.8 μm) and α_2 (11.0 μm) grains than those in Al6Cu and Al10Cu alloys.

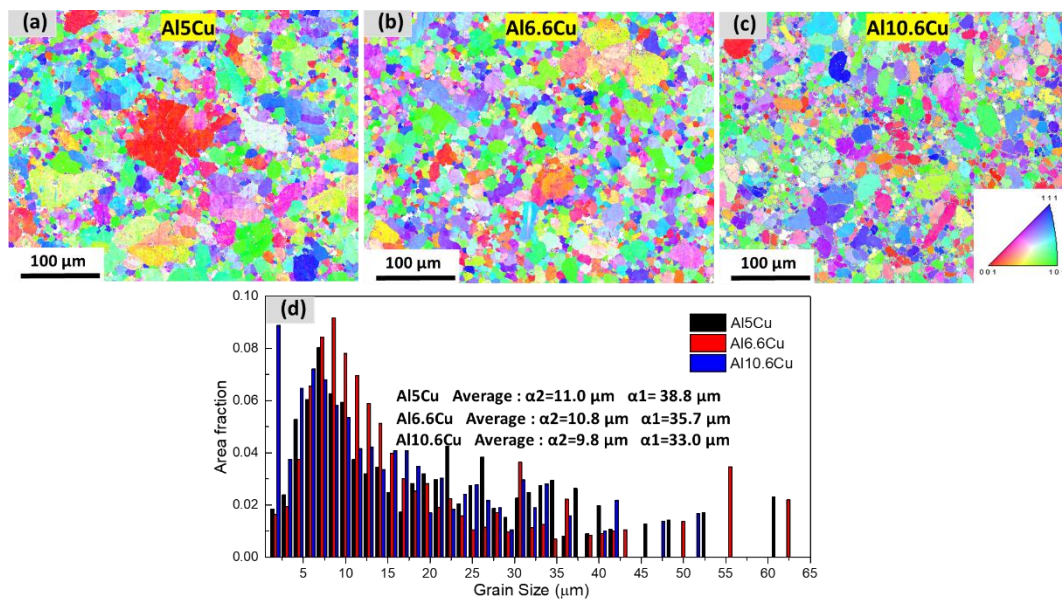


Fig.5 EBSD orientation map of α -Al grains in Al5Cu (a), Al6.6Cu (b), Al10.6Cu (c) and corresponding grain size distribution (d)

Fig.6 (a-b) shows the ultrafine eutectic microstructure in Al5Cu alloy. It consisted of four phases (e.g. Al_2Cu , Si, Q and α -Al) as confirmed by selected electron diffraction patterns, as shown in Fig 6 (c-f). Such ultrafine eutectic mixture was also found in Al6.6Cu by TEM analysis and the TEM result for Al6.6Cu is not included here. The α -Al and Al_2Cu phases co-existed together in a lamellar structure with a lamellar spacing of 100-250 nm, which is slightly finer than that in Al10.6Cu alloy. Q phase shows irregular morphology without attaching to Al_2Cu lamellas. Fine Si particles were found in the ultrafine eutectic region as well, and there are no orientation relationships among these phases.

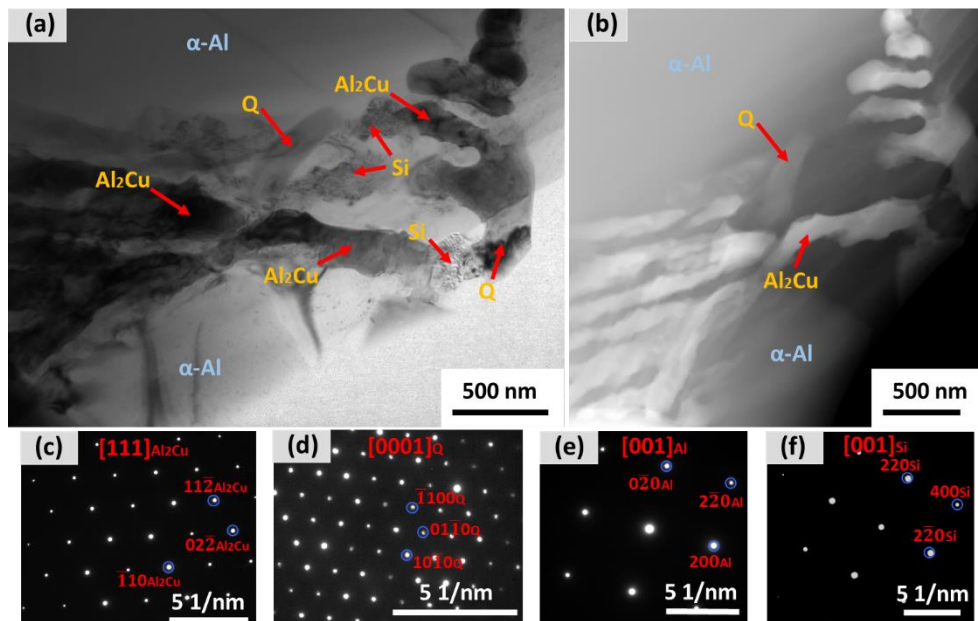


Fig.6 (a) TEM bright-field image (b) HAADF-STEM image showing the ultrafine eutectic region in Al5Cu (c-f) SADP patterns of Al_2Cu , Q, α -Al and Si

Fig.7 shows the ultrafine eutectic microstructure of Al10.6Cu. The TEM bright-field image (Fig.7. (a)) is taken along the $[110]_{\text{Al}_2\text{Cu}}$ zone axis, and the fine eutectic mixture consisted of a mixture of four phases (e.g. Al_2Cu , Si, Q and α -Al). The Al_2Cu and α -Al eutectic mixture exhibit a lamellar structure with an interlamellar spacing in the range of 150nm to 300 nm, and all Q phase particles are attached to the Al_2Cu lamella. Only one particle of Si phase was observed in this quaternary eutectic region, which is marked in Fig.7 (a). The EDX mapping of Area 1 in Fig.7 (a) is shown in Fig.7 (b). The X-ray mapping was used to indicate elemental components of each phase present in the microstructure and subsequent identification of each phase was performed

using selected area electron diffraction patterns obtained from TEM studies. All spherical particles in Fig.7 (a) are found to be Q phase, and the size distribution is 50-100 nm. The SADP patterns of Q, Al₂Cu, Si and α-Al phases are shown in Fig.7 (c-f). The 3D analysis of the morphology of eutectic phases was carried out with FIB-SEM tomography, as shown in Video (S1). The Q phase shows a fibrous morphology and attaches itself to the Al₂Cu lamellae, while the Si phase exhibits irregular morphology with a small area fraction entrapped between the Al₂Cu lamellae.

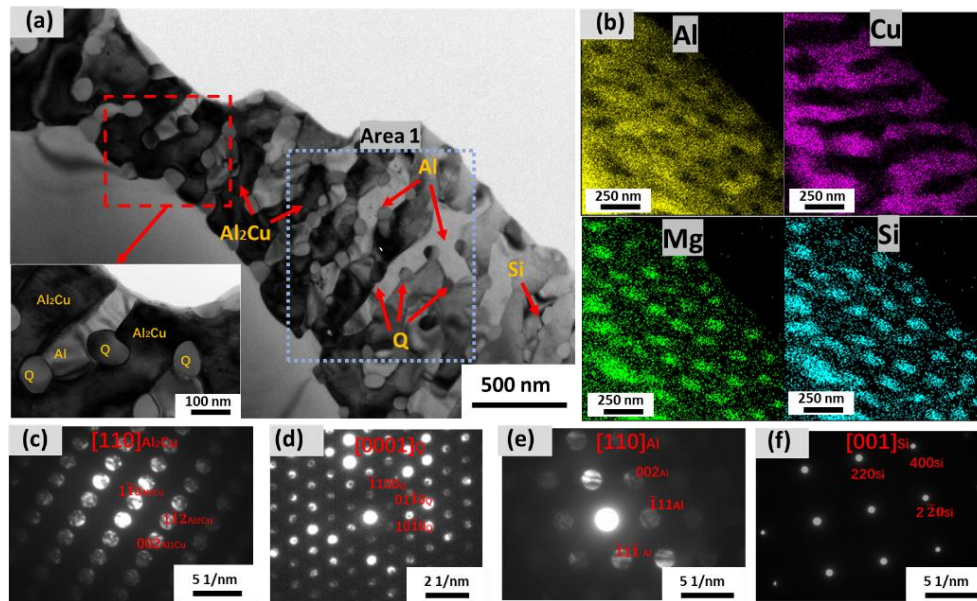


Fig.7 (a) TEM bright-field image with the inserted high-magnified image showing the ultrafine eutectic region in Al_{10.6}Cu (b) corresponding X-ray elemental maps obtained from the rectangular 'Area 1' (c-f) SADP patterns of Al₂Cu, Q, α-Al and Si

The orientation relationships between each of Al₂Cu, Q and α-Al phases in Al_{10.6}Cu alloy were determined from HRTEM studies of eutectic phases shown in Fig.7 (a). Fig.8 shows HRTEM images and corresponding FFT patterns, as well as one-dimensional Fourier-filtered images of interfaces between the eutectic phases. Fig.8 (a) shows the interface structure between Al₂Cu and α-Al. From the corresponding FFT in Fig.8 (b), the orientation relationship between α-Al and Al₂Cu was found to be $(\bar{2}20)_{Al} \sim 3^\circ \text{ from } (00\bar{2})_{Al_2Cu}$ and $[110]_{Al} // [110]_{Al_2Cu}$. The HRTEM image and FFT of the interface structure between Q and α-Al are shown in Fig.8 (d,e), respectively. The parallel planes of Q and α-Al were identified to be $(\bar{1}13)_{Al}$ and $(10\bar{1}0)_Q$ from FFT pattern. The orientation relationship between Q and α-Al was found to be $[110]_{Al} // [0001]_Q$ and $(\bar{1}13)_{Al} // (10\bar{1}0)_Q$. The orientation relationship between Al₂Cu and Q was

determined from Fig.8 (g) and (h). The angle between $(00\bar{2})_{Al_2Cu}$ and $(\bar{1}100)_Q$ planes are $\sim 3^\circ$ when $[110]_{Al_2Cu} // [0001]_Q$. Hence, the orientation relationships between Al_2Cu , Q, and α -Al is summarised as:

$$\left\{ \begin{array}{l} (\bar{2}20)_{Al} \sim 3^\circ \text{ from } (00\bar{2})_{Al_2Cu}, (\bar{1}13)_{Al} / (10\bar{1}0)_Q, (00\bar{2})_{Al_2Cu} \sim 3^\circ \text{ from } (\bar{1}100)_Q \\ [110]_{Al} // [110]_{Al_2Cu} // [0001]_Q \end{array} \right.$$

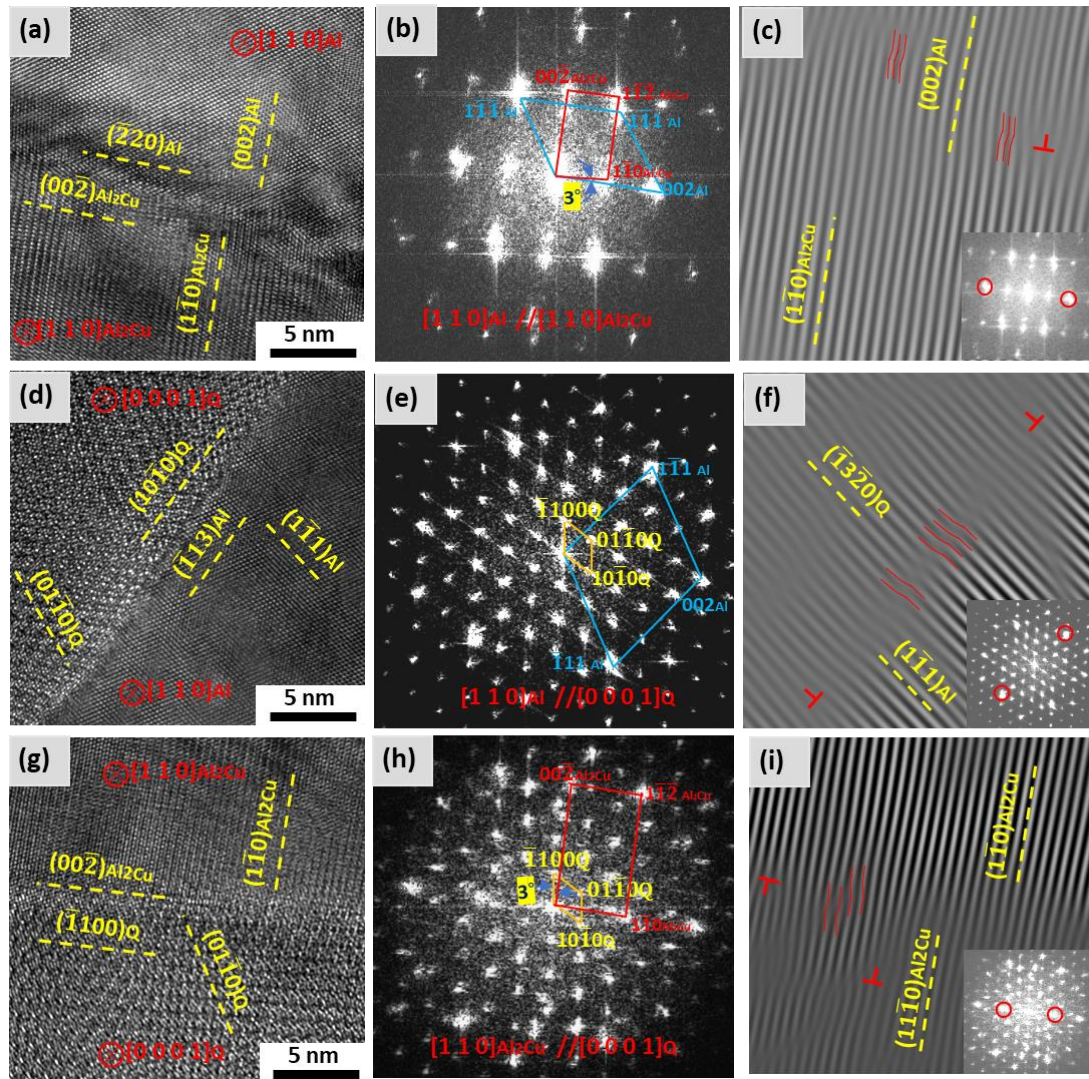


Fig.8 (a, d, g) HRTEM image showing the interface of Al and Al_2Cu , Q and Al, Al_2Cu and Q in $Al_{10.6}Cu$, respectively (b, e, h) fast Fourier transformation (FFT) image of their HRTEM (c, f, i) Fourier transformed patterns of the interfaces between the eutectic phases

Fig.8 (c,f,i) shows one-dimensional Fourier-filtered images of boundaries between these eutectic phases. Dislocations on the interfaces among these three phases were observed. There are only a few dislocations found between

α -Al and Al₂Cu interface, which indicates a coherent interface. Such interfaces are very stable and cannot easily be modified. However, there is a larger amount of distortion between Q and Al₂Cu, α -Al and Q interfaces, in which different types of dislocations coexist.

3.3 Mechanical properties

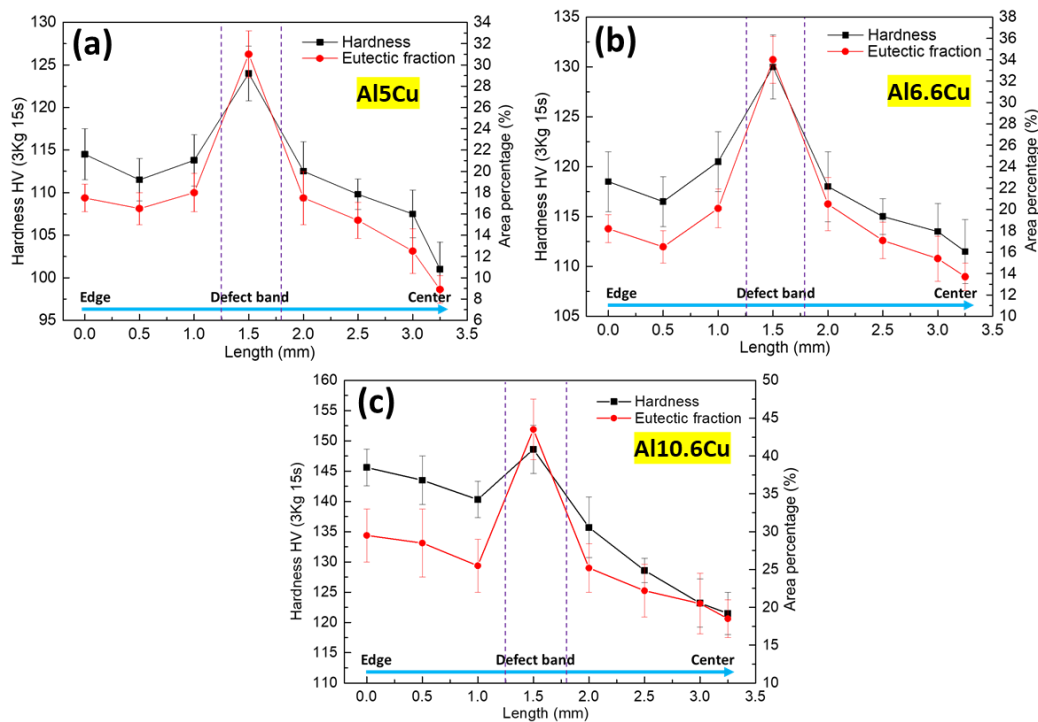


Fig.9 The average hardness and area percentage of eutectic mixtures from the edge to the centre of the tensile sample (a) Al5Cu (b) Al6.6Cu and (c) Al10.6Cu

Fig.9 shows the average hardness and area percentage of the eutectic mixture in these three alloys which were obtained from the edge to the centre of the cross-section. The area percentage of the eutectic mixture was measured from the backscattered SEM images using an ImageJ software. The central region of each alloy contained the lowest area percentage of the eutectic mixture, while the defect band region has the highest volume fraction of eutectic mixture. The hardness profile for each alloy coincides with the profile of area percentage of the eutectic mixture from the centre to the edge region. The highest hardness in Al10.6Cu alloy was achieved to be 147 HV in the defect band region, and the hardness in the central region is about 120 HV. Al5Cu alloy has the lowest hardness of 101 HV in the central region with the least amount of area percentage of eutectic mixture of 8.9%.

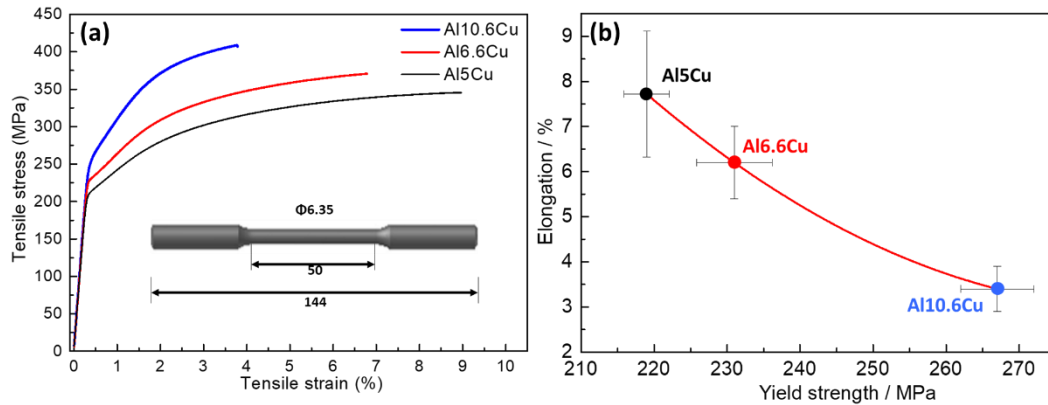


Fig.10 The tensile stress-strain curves of die-cast quaternary Al-Cu-Si-Mg hypoeutectic alloys

Fig.10 (a) shows the tensile stress-strain curves of these three alloys, and an inset of a typical standard tensile test sample. Table 3 compares tensile properties of alloys studied in this work with those found in recently developed die-cast alloys. The quaternary Al-Cu-Si-Mg hypoeutectic alloys show excellent mechanical properties with a good combination of strength and ductility. Al10.6Cu alloy has the highest yield strength of 267 ± 5 MPa and ultimate tensile strength of 395 ± 16 MPa, but the lowest elongation of $3.4 \pm 0.5\%$. The ultimate tensile strength of Al10.6Cu far exceeds the ultimate tensile strength (e.g. below 350MPa) of existing die-cast alloys reported in the literature. However, the highest elongation of $7.72 \pm 1.4\%$ was found in Al5Cu with good yield strength of 219 ± 3.1 MPa and ultimate tensile strength of 344.7 ± 6.5 MPa. The Al-Cu-Si-Mg die-cast alloys exhibit a yield strength above 200 MPa and a good elongation to failure, which can be tailored by modification of the percentage of eutectic mixture. Fig.10.(b) shows a plot of elongation versus yield strength of these three alloys. The measured area percentages of eutectic mixture in Al5Cu, Al6.6Cu and Al10.6Cu are 17.1%, 21.4% and 26.6%, respectively. The increase in area percentage of the eutectic mixture from 21.4% in Al6.6Cu alloy to 26.6% in Al10.6Cu leads to a dramatic increase in the yield strength and a reduction in the elongation to failure to a useful level of 3.4%.

Table 3 The mechanical properties of the recently developed die-cast alloys and the alloys studied in this work

Alloy composition(wt%)	Temper	Tensile Strength/MPa	Yield Strength /MPa	Elongation /%
Al10Si1.2Cu0.8Mn [36]	As-cast	308	190	6.6
Al10Si0.4Mg0.55Fe0.2-0.85Mn [37]	As-cast	~225	~150	8-12
Al7Si0.7Mn0.3Mg [38]	As-cast	~260	~125	~10
Al9Si3Cu [39]	As-cast	~330	~140	~6
Al5.5Mg2Si0.57Mn [1]	As-cast	~320	~180	~8
Al10Mg2.8Si3.5Zn0.5Mn [2]	As-cast	~350	~250	~2.0
Al8Si3Cu1.8Zn0.86Fe [40]	As-cast	~339	~147	~5.2
Al10Si1.6Cu0.68Fe [41]	As-cast	~300	~213	~1.8
Current Work	Al5Cu	344.7±6.5	219±3.1	7.72±1.4
	Al6.6Cu	365±4.5	231±5.2	6.2±0.8
	Al10.6Cu	395±16	267±5	3.4±0.5

The fracture surfaces of these three alloys are shown in Fig.11. From Fig.11, a combination of eutectic separation and cleavage fracture of α_1 -Al grains, as well as some porosities can be found. More eutectic separation appeared in Al10.6Cu (Fig.11 (c)), corresponding to the highest area percentage of the eutectic mixture. A few dimple ruptures were found in α_2 -Al regions in Al5Cu and Al6.6Cu, indicating the higher ductility.

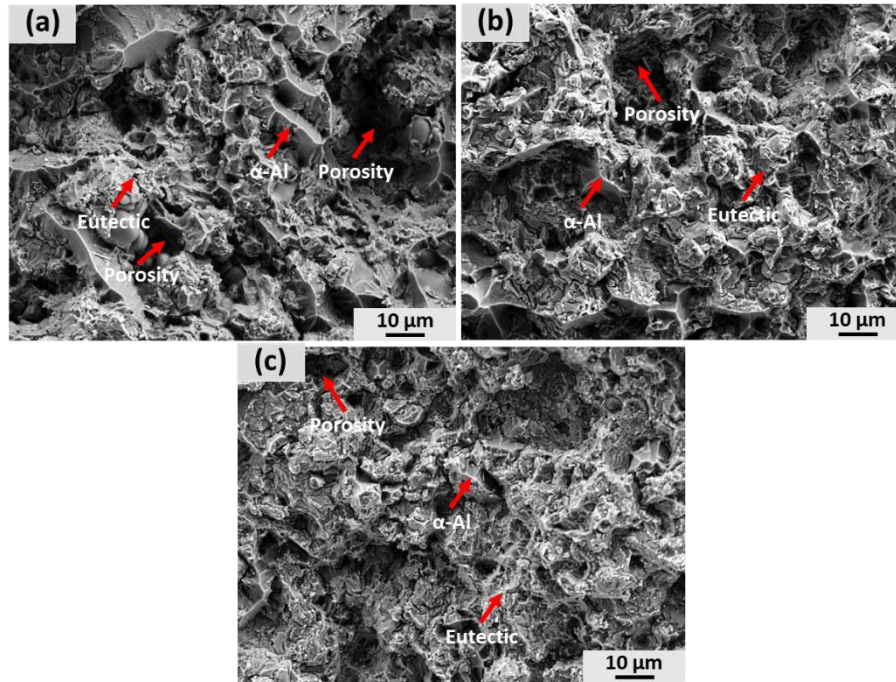


Fig.11 SEM micrographs showing fracture surfaces of Al5Cu (a), Al6.6Cu (b) and Al10.6Cu (c)

4. Discussion

4.1 Microstructure evolution

Solidification during HPDC process is a two-stage solidification process, which commences when the melt is poured into the shot sleeve. The relatively low temperature of the shot sleeve (250 °C) is able to cool the melt below the liquidus temperature [42], and the α_1 -Al grains initiate a start forming in the shot sleeve. After passing through the narrow ingate, the fragmented or rosette α_1 -Al grains form. During the filling process in the die cavity, much finer α_2 -Al grains form, due to the high cooling rate ~ 1000 K/s [43]. With increasing Cu content, both α_1 -Al and α_2 -Al grains becomes finer. Al10.6Cu has the finest grain size, due to the growth restriction as the increased amount of solute in the solid/liquid front mitigates the dendritic growth [44].

A defect band can be observed in die-cast alloys, as a result of macrosegregation of alloying elements associated with high Cu containing alloy composition and high percentage of the eutectic mixture. The mechanism of defect band formation was proposed by Gourlay et al [45]. It is because of the dilatant shear bands resulting from strain instabilities of initially solidified grains

[45]. In addition, the accompanied macrosegregation in the defect band region is due to the inverse segregation or exudation [46].

Furthermore, the addition of Mn can suppress the formation of needle-like β -AlFeSi phase, and the small addition of Fe and high cooling rates contribute to the fine α -AlFeMnSi particles, which form prior to eutectic reactions. Most of the α -AlFeMnSi particles are distributed along the grain boundaries. Thus, the minor addition of Mn and Fe have minimal effect on the types of eutectic phases formed during solidification.

The formation of ultrafine quaternary eutectic structures in Al5Cu, Al6.6Cu and Al10.6Cu alloys occurs at the end of the solidification in HPDC process. Al10.6Cu alloy, which was designed with quaternary hypoeutectic composition, has uniform eutectic microstructure. The reduction of Cu content in Al-Cu-Si-Mg alloy can decrease the total volume fraction of eutectic mixture, and some binary or ternary eutectic structures are formed at high temperature with a coarser morphology. The final quaternary eutectic in these three alloys exhibits a very fine microstructure. The solidification of a multi-phase quaternary eutectic mixture occurs via competitive growth process and cooperative/decoupled growth of eutectic phases [12]. Thus, compared with binary or ternary eutectic reactions, the solute diffusion across the solid/liquid interface of quaternary eutectic mixture is more complex, and is accompanied by high constitutional undercooling. Therefore, the lamellar thickness or spacing of multi-component eutectic alloys is usually finer than their binary counterparts.

Moreover, the final quaternary eutectic microstructure involves the coupled growth of α -Al, Q and Al₂Cu phases and the independent growth of the facet Si phase, as observed in Al10.6Cu alloy. However, in Al5Cu and Al6.6Cu, the morphology is different, and only coupled growth of α -Al and Al₂Cu eutectic phases without any cooperative growth of Q phase attaching the lamellae. There is a large variation in the interfacial energy associated with Q phase due to the hexagonal crystal structure, whereas the coupled growth of these three phases is very difficult and only occurs at specific undercooling conditions. Meanwhile, the smaller interdendritic regions in Al5Cu and Al6.6Cu alloys represent solidification at a higher cooling rate as compared that in Al10Cu, which was indicated by finer lamellar spacing. Consequently, the high cooling rate in the HPDC of Al5Cu and Al6.6Cu is believed to prevent the cooperative growth of Q phase with α -Al and Al₂Cu.

The interfaces among α -Al, Q and Al₂Cu phases were well defined from HRTEM studies of Al10.6Cu. Bramfitt [47] calculated the misfit of the interfaces where lattice mismatch (δ) can be expressed as:

$$\delta = \sum_{i=1}^3 \frac{|(d_{[uvw]_s^i} \cos \theta) - d_{[uvw]_n^i}|}{d_{[uvw]_n^i}} \times 100$$

where $[uvw]_n^i$ is the low-index direction of one phase, $[uvw]_s^i$ is the low-index direction of another phase, $d_{[uvw]_s^i}$ is the d-spacing along $[uvw]_s^i$

direction and $d_{[uvw]_n^i}$ is the d-spacing along $[uvw]_n^i$ direction. The mismatch between the interfaces was reconstructed and simulated based on Bramfitt method. Fig.12 shows the atomic matching of the common planes among Al_2Cu , Q and $\alpha\text{-Al}$ phases. The selection of common planes and zone axis directions is based on results shown in Fig.7. The calculation parameters are listed in Supplementary Material (Table S1).

The interface between Q and Al_2Cu has the highest δ value of 7.3%, while the δ value of interface between $\alpha\text{-Al}$ and Al_2Cu is smallest (2.3%). Based on the authors' knowledge, the orientation described is a new orientation relationship for $\alpha\text{-Al}\text{-Al}_2\text{Cu}$, which formed a coherent interface during solidification. This orientation relationship is different from that in binary $\text{Al}\text{-Cu}$ or ternary $\text{Al}\text{-Cu}\text{-Ag}$ systems [48,49]. The interfaces of Q and Al_2Cu , as well as Q and $\alpha\text{-Al}$, are semi-coherent. The common interfaces between phases are usually found in the eutectic solidification to facilitate the reduction of the total energy of the system. In this alloy, a majority of interfaces are formed between $\alpha\text{-Al}$ and Al_2Cu lamellae. The interfacial energy of Q/ Al_2Cu and Q/ $\alpha\text{-Al}$ is higher than $\alpha\text{-Al}/\text{Al}_2\text{Cu}$. The lowest mismatch between $\alpha\text{-Al}$ and Al_2Cu and lowest interfacial strain in Q/ Al_2Cu and Q/ $\alpha\text{-Al}$ interfaces enable the development of the orientation relationship among three eutectic phases. However, the nucleation and coupled growth mechanism of this quaternary eutectic system still need to be further systematically studied.

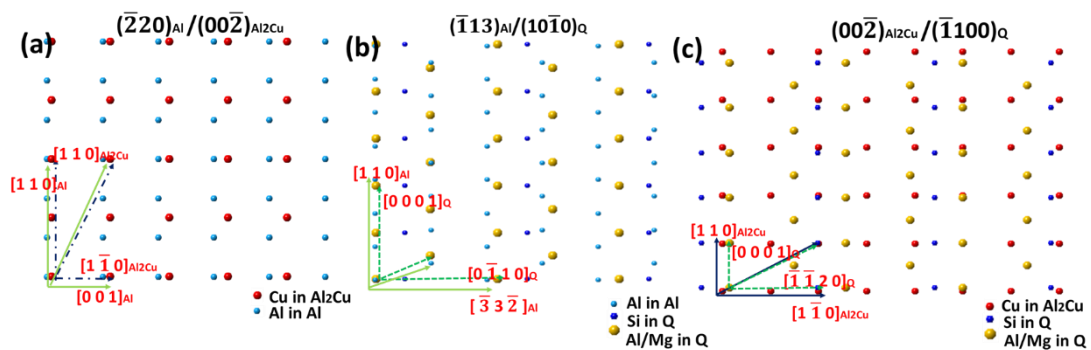


Fig.12 Schematic illustration of the matching of interfaces for $(\bar{2}20)_{Al}$ / $(00\bar{2})_{Al_2Cu}$ (a), $(\bar{1}13)_{Al}$ / $(10\bar{1}0)_Q$ (b) and $(00\bar{2})_{Al_2Cu}$ / $(\bar{1}100)_Q$ (c) respectively

4.2 Relationship between microstructure and mechanical properties

Table 3 compares the tensile properties of recently reported die-cast alloys based on Al-Si, or Al-Mg binary systems with those obtained from quaternary Al-Cu-Si-Mg hypoeutectic alloys. The newly developed Al5Cu and Al6.6Cu alloys have comparable tensile properties to existing die-cast alloys. However, Al10.6Cu alloy has superior tensile properties to those of reported die-cast alloys. The strengthening mechanism of current die-cast alloys is contributed by eutectic phases, such as Si or Mg₂Si. Some Fe and Mn are added into these existing alloys, forming α -AlFeMnSi intermetallic compound, which further enhances the strength of these alloys. Moreover, it was found that the addition of Cu into Al-Si alloys or addition of Zn into Al-Mg alloys lead to the yield strength close to or greater than 200 MPa, due to a combination of solute solution strengthening of α -Al and second phase strengthening of copper-/zinc-contained intermetallic compound [2,36,41]. Although these die-cast alloys have yield strengths close to or over 200 MPa, the elongation to failure is relatively small (e.g. below 3%), resulting from increased volume fraction of copper-/zinc-contained intermetallic compounds [2,36,40,41].

The microstructure of quaternary Al-Cu-Mg-Si hypoeutectic alloys consists of ultrafine quaternary eutectic mixture, compact α -AlFeMnSi particles and fine α -Al grains. The fine size and morphology of α -AlFeMnSi phases with considerably low volume fraction have little negative influence on crack initiation [37]. Moreover, the Al₂Cu phase, which is the majority of intermetallic compound inside the eutectic region, has high elasticity [50] and forms a fine lamellar structure with α -Al phase. Thus, a large interaction force is required for the generation of dislocations in the lamellae [50]. Additional strengthening mechanism is contributed from other fine eutectic phases such as fibrous Q and irregular Si phases. Consequently, the alloys in the current work show more favourable mechanical properties than existing die-cast alloys.

The volume fraction of eutectic mixture plays a vital role in the elongation and strength of the alloys [5]. Okulov et al. reported that during deformation of hypoeutectic ultrafine eutectic alloys, the microstructure undergoes three stages [21]. The wave slip bands form, which is caused by dislocation pile-ups, and it is usually observed along a closed packed plane. After that, the slip bands increases and penetrate into ultrafine regions. With further deformation, cracks

are formed in the eutectic regions and propagate along with the slip bands, resulting in final failure. With the increase in the volume fraction of eutectic mixture more interconnected ultrafine eutectic mixture in the alloy is able to retard the deformation of soft α -Al dendrites. Consequently, this results in excellent yield strength and ultimate tensile strength properties, but lower elongation to failure. Moreover, with further deformation, the dendrites cannot accommodate the tensile stress, resulting in fast propagation of cracks along grain boundaries. The failure occurs as a result of the separation of interdendritic eutectic region .

Lastly, the relationship between yield strength and elongation is nonlinear. As shown in Fig.10 (b), the increasing Cu content in the Al-Cu-Si-Mg alloy composition leads to an increase in the area percentage of eutectic mixture and strength but a decrease in elongation to failure. Compared with Al5Cu and Al6.6Cu, Al10.6Cu has a uniform ultrafine eutectic structure without any coarse binary or ternary eutectic mixture. In the meantime, this quaternary ultrafine eutectic with a fine lamellar morphology can effectively dissipate the excessive strain in the form of multi-cracks [51]. In addition, the interfaces between α -Al and Al₂Cu are coherent, which is favourable for dislocation propagation [52]. To summarise, the approach of designing alloys with multi-phase and multi-component eutectic structure concept offers huge potential for alloy development with exceptional strength and acceptable ductility.

5. Conclusions

- (1) The die-cast Al-Cu-Si-Mg alloys with designed 20-30% ultrafine eutectic mixture show excellent yield strength of 219-267 MPa, ultimate tensile strength 344.7-395 MPa and elongation of 3.4-7.72 %, respectively.
- (2) The microstructure of Al5Cu and Al6.6Cu alloys mainly consists of fine α -Al phases, binary/ternary eutectic and quaternary eutectic mixture (Si, Al₂Cu, α -Al and Al₄Cu₂Mg₈Si₇). The Al10.6Cu alloy has a uniform ultrafine quaternary eutectic (Si, Al₂Cu, α -Al and Al₄Cu₂Mg₈Si₇) with the absence of coarse binary/ternary eutectic structure.
- (3) The Al10.6Cu has the smallest α 1-Al and α 2-Al grain sizes compared with those in Al5Cu and Al6Cu alloys. The α 1-Al and α 2-Al grain increase in size with decreasing Cu content in the alloy composition.
- (4) The defect band region has the highest area percentage of eutectic mixtures, as well as the highest hardness in each alloy.
- (5) The coupled growth of Al₂Cu, α -Al and Q(Al₄Cu₂Mg₈Si₇) phases was found in Al10.6Cu alloy. The α -Al-Al₂Cu lamellae exhibit coherent an interface, while the α -Al-Q and Al₂Cu-Q interfaces are semi-coherent. This orientation relationship of the quaternary eutectic phases is absent in Al5Cu and

Al6.6Cu alloys due to the different solidification condition, as compared to that in Al10.6Cu.

Acknowledgements

The authors gratefully acknowledge support from the Engineering and Physical Sciences Research Council (EPSRC) for the financial support on Future Liquid Metal Engineering (LiME) Hub (EP/N007638/1). Qing Cai is very grateful to Brunel University London for the financial support on his PhD studies. The authors would thank Experimental Techniques Centre Brunel University London for access to the characterisation facilities.

Data availability

The raw/processed data required to reproduce these findings cannot be shared at a public repository at this time as the data also forms part of an ongoing study.

References

- [1] Z. Hu, L. Wan, S. Wu, H. Wu, X. Liu, Microstructure and mechanical properties of high strength die-casting Al–Mg–Si–Mn alloy, *Mater. Des.* 46 (2013) 451–456. <https://doi.org/10.1016/j.matdes.2012.10.020>.
- [2] S. Ji, F. Yan, Z. Fan, Development of a high strength Al–Mg₂Si–Mg–Zn based alloy for high pressure die casting, *Mater. Sci. Eng. A.* 626 (2015) 165–174. <https://doi.org/10.1016/j.msea.2014.12.019>.
- [3] F. Bonollo, N. Gramegna, G. Timelli, High-pressure die-casting: Contradictions and challenges, *JOM.* 67 (2015) 901–908. <https://doi.org/10.1007/s11837-015-1333-8>.
- [4] J.H. Han, K.B. Kim, S. Yi, J.M. Park, D.H. Kim, S. Pauly, J. Eckert, Influence of a bimodal eutectic structure on the plasticity of a (Ti 70.5 Fe29.5)₉₁ Sn₉ ultrafine composite, *Appl. Phys. Lett.* 93 (2008) 1–4. <https://doi.org/10.1063/1.3029745>.
- [5] Q. Cai, C.L. Mendis, I.T.H. Chang, Z. Fan, Microstructure evolution and mechanical properties of new die-cast Al–Si–Mg–Mn alloys, *Mater. Des.* 187 (2020) 108394. <https://doi.org/10.1016/j.matdes.2019.108394>.

- [6] E.M. Park, C.H. Lee, J.M. Park, J.H. Han, G.A. Song, J.T. Kim, S.H. Hong, J.Y. Park, Y. Seo, N.S. Lee, K.B. Kim, Heterogeneous duplex structured Ti-Sn-Mo alloys with high strength and large plastic deformability, *J. Alloys Compd.* 574 (2013) 546–551. <https://doi.org/10.1016/j.jallcom.2013.05.061>.
- [7] J.M. Park, K.B. Kim, D.H. Kim, N. Mattern, R. Li, G. Liu, J. Eckert, Multi-phase Al-based ultrafine composite with multi-scale microstructure, *Intermetallics*. 18 (2010) 1829–1833. <https://doi.org/10.1016/j.intermet.2010.02.042>.
- [8] N. Hua, F. Yue, Ultrafine-structured Ni-based bulk alloys with high strength and enhanced ductility, *Mater. Sci. Eng. A*. 692 (2017) 17–23. <https://doi.org/10.1016/j.msea.2017.03.019>.
- [9] Y.S. Kim, H.J. Park, J.T. Kim, S.H. Hong, G.H. Park, J.M. Park, J.Y. Suh, K.B. Kim, Influence of Nb on microstructure and mechanical properties of Ti-Sn ultrafine eutectic alloy, *Met. Mater. Int.* 23 (2017) 20–25. <https://doi.org/10.1007/s12540-017-6263-2>.
- [10] J.Y. Lee, K.H. Han, J.M. Park, K. Chattopadhyay, W.T. Kim, D.H. Kim, Deformation and evolution of shear bands under compressive loading in bulk metallic glasses, *Acta Mater.* 54 (2006) 5271–5279. <https://doi.org/10.1016/j.actamat.2006.07.014>.
- [11] D. Jia, K.T. Ramesh, E. Ma, Effects of nanocrystalline and ultrafine grain sizes on constitutive behavior and shear bands in iron, *Acta Mater.* 51 (2003) 3495–3509. [https://doi.org/10.1016/S1359-6454\(03\)00169-1](https://doi.org/10.1016/S1359-6454(03)00169-1).
- [12] B. Chanda, G. Potnis, P.P. Jana, J. Das, A review on nano-/ultrafine advanced eutectic alloys, *J. Alloys Compd.* 827 (2020) 154226. <https://doi.org/10.1016/j.jallcom.2020.154226>.
- [13] J.M. Park, N. Mattern, U. Kuhn, J. Eckert, K.B. Kim, W.T. Kim, K. Chattopadhyay, D.H. Kim, High-strength bulk Al-based bimodal ultrafine eutectic composite with enhanced plasticity, *J. Mater. Res.* 24 (2011) 2605–2609. <https://doi.org/10.1557/jmr.2009.0297>.
- [14] C.S. Tiwary, S. Kashyap, K. Chattopadhyay, Development of alloys with high strength at elevated temperatures by tuning the bimodal microstructure in the Al-Cu-Ni eutectic system, *Scr. Mater.* 93 (2014) 20–23. <https://doi.org/10.1016/j.scriptamat.2014.08.020>.

- [15] J.T. Kim, S.H. Hong, J.M. Park, J. Eckert, K.B. Kim, Microstructure and mechanical properties of hierarchical multi-phase composites based on Al-Ni-type intermetallic compounds in the Al-Ni-Cu-Si alloy system, *J. Alloys Compd.* 749 (2018) 205–210. <https://doi.org/10.1016/j.jallcom.2018.03.313>.
- [16] C.H. Lee, S.H. Hong, J.T. Kim, H.J. Park, G.A. Song, J.M. Park, J.Y. Suh, Y. Seo, M. Qian, K.B. Kim, Chemical heterogeneity-induced plasticity in Ti-Fe-Bi ultrafine eutectic alloys, *Mater. Des.* 60 (2014) 363–367. <https://doi.org/10.1016/j.matdes.2014.03.048>.
- [17] G.A. Song, W. Lee, N.S. Lee, K.B. Kim, J.M. Park, D.H. Kim, J. Lee, J.S. Park, Microstructural evolution and mechanical properties of Mg-Cu-Zn ultrafine eutectic composites, *J. Mater. Res.* 24 (2009) 2892–2898. <https://doi.org/10.1557/jmr.2009.0330>.
- [18] S. Samal, S. Agarwal, K. Biswas, Phase Evolution and Mechanical Properties of Suction Cast Ti-Fe-Co Ternary Alloys, *Trans. Indian Inst. Met.* (2017). <https://doi.org/10.1007/s12666-017-1174-y>.
- [19] J.M. Park, D.H. Kim, K.B. Kim, J. Eckert, Improving the plasticity of a high strength Fe-Si-Ti ultrafine composite by introduction of an immiscible element, *Appl. Phys. Lett.* 97 (2010) 1–4. <https://doi.org/10.1063/1.3532100>.
- [20] E.M. Park, G.A. Song, J.H. Han, Y. Seo, J.Y. Park, K.B. Kim, Solid-state phase transformation-induced heterogeneous duplex structure in Ti-Sn-Fe alloys, *J. Alloys Compd.* 515 (2012) 86–89. <https://doi.org/10.1016/j.jallcom.2011.11.078>.
- [21] I. V. Okulov, M. Bonisch, U. Kuhn, W. Skrotzki, J. Eckert, Significant tensile ductility and toughness in an ultrafine-structured Ti68.8Nb13.6Co6Cu5.1Al6.5 bi-modal alloy, *Mater. Sci. Eng. A.* 615 (2014) 457–463. <https://doi.org/10.1016/j.msea.2014.07.108>.
- [22] C. Yang, L.M. Kang, X.X. Li, W.W. Zhang, D.T. Zhang, Z.Q. Fu, Y.Y. Li, L.C. Zhang, E.J. Lavernia, Bimodal titanium alloys with ultrafine lamellar eutectic structure fabricated by semi-solid sintering, *Acta Mater.* 132 (2017) 491–502. <https://doi.org/10.1016/j.actamat.2017.04.062>.
- [23] J.M. Park, K.B. Kim, W.T. Kim, M.H. Lee, J. Eckert, D.H. Kim, High strength ultrafine eutectic Fe-Nb-Al composites with enhanced plasticity, *Intermetallics.* 16 (2008) 642–650.

- <https://doi.org/10.1016/j.intermet.2008.01.005>.
- [24] Y. Kaygisiz, N. Marasli, Directional solidification of Al-Cu-Si-Mg quaternary eutectic alloy, *J. Alloys Compd.* 721 (2017) 764–771. <https://doi.org/10.1016/j.jallcom.2017.06.027>.
- [25] H. Kaya, E. Cadirli, M. Gunduz, A. Ulgen, Effect of the temperature gradient, growth rate, and the interflake spacing on the microhardness in the directionally solidified Al-Si eutectic alloy, *J. Mater. Eng. Perform.* 12 (2003) 544–551. <https://doi.org/10.1361/105994903100277201>.
- [26] Y. Kaygisiz, N. Marasli, Microstructural, mechanical and electrical characterization of directionally solidified Al-Si-Mg eutectic alloy, *J. Alloys Compd.* 618 (2015) 197–203. <https://doi.org/10.1016/j.jallcom.2014.08.056>.
- [27] U. Boyuk, Physical and mechanical properties of Al-Si-Ni eutectic alloy, *Met. Mater. Int.* 18 (2012) 933–938. <https://doi.org/10.1007/s12540-012-6004-5>.
- [28] S. Engin, U. Buyuk, N. Marasli, The effects of microstructure and growth rate on microhardness, tensile strength, and electrical resistivity for directionally solidified Al-Ni-Fe alloys, *J. Alloys Compd.* 660 (2016) 23–31. <https://doi.org/10.1016/j.jallcom.2015.11.080>.
- [29] L. Wang, M. Makhlouf, D. Apelian, Aluminium die casting alloys: alloy composition, microstructure, and properties-performance relationships, *Int. Mater. Rev.* 40 (1995) 221–238. <https://doi.org/10.1179/imr.1995.40.6.221>.
- [30] J.R. Galvele, S.M. de De Micheli, Mechanism of intergranular corrosion of Al-Cu alloys, *Corros. Sci.* 10 (1970) 795–807. [https://doi.org/10.1016/S0010-938X\(70\)80003-8](https://doi.org/10.1016/S0010-938X(70)80003-8).
- [31] X. ZHANG, J. SUN, M. WANG, Y. ZHANG, N. MA, H. WANG, Improvement of yttrium on the hot tearing susceptibility of 6TiB2/Al-5Cu composite, *J. Rare Earths.* 33 (2015) 1335–1340. [https://doi.org/10.1016/S1002-0721\(14\)60566-4](https://doi.org/10.1016/S1002-0721(14)60566-4).
- [32] L.F Mondolfo, *Aluminum Alloys Structure and Properties*, 1976. <https://books.google.com/books?hl=en&lr=&id=Xf4kBQAAQBAJ&oi=fnd&pg=PP1&ots=Q54C0qKuqb&sig=imOmvIPGFhWsr8ir24rMKU7Ve5g> (accessed January 22, 2020).

- [33] S. Ji, W. Yang, F. Gao, D. Watson, Z. Fan, Effect of iron on the microstructure and mechanical property of Al–Mg–Si–Mn and Al–Mg–Si diecast alloys, *Mater. Sci. Eng. A.* 564 (2013) 130–139. <https://doi.org/10.1016/j.msea.2012.11.095>.
- [34] H. Zhu, J. Guo, J. Jia, Experimental study and theoretical analysis on die soldering in aluminum die casting, *J. Mater. Process. Technol.* 123 (2002) 229–235. [https://doi.org/10.1016/S0924-0136\(01\)01174-8](https://doi.org/10.1016/S0924-0136(01)01174-8).
- [35] A.R. Adamane, L. Arnberg, E. Fiorese, G. Timelli, F. Bonollo, Influence of injection parameters on the porosity and tensile properties of high-pressure die cast Al-Si alloys: A review, *Int. J. Met.* 9 (2015) 43–52. <https://doi.org/10.1007/bf03355601>.
- [36] P. Zhang, Z. Li, B. Liu, W. Ding, Effect of chemical compositions on tensile behaviors of high pressure die-casting alloys Al-10Si-yCu-xMn-zFe, *Mater. Sci. Eng. A.* 661 (2016) 198–210. <https://doi.org/10.1016/j.msea.2016.03.032>.
- [37] D. Bosch, S. Pogatscher, M. Hummel, W. Fragner, P.J. Uggowitzer, M. Goken, H.W. Hoppel, Secondary Al-Si-Mg High-pressure Die Casting Alloys with Enhanced Ductility, *Metall. Mater. Trans. A Phys. Metall. Mater. Sci.* 46 (2015) 1035–1045. <https://doi.org/10.1007/s11661-014-2700-8>.
- [38] G. Timelli, O. Lohne, L. Arnberg, H.I. Laukli, Effect of Solution Heat Treatments on the Microstructure and Mechanical Properties of a Die-Cast AlSi7MgMn Alloy, *Metall. Mater. Trans. A.* 39 (2008) 1747–1758. <https://doi.org/10.1007/s11661-008-9527-0>.
- [39] G. Timelli, F. Bonollo, The influence of Cr content on the microstructure and mechanical properties of AlSi9Cu3(Fe) die-casting alloys, *Mater. Sci. Eng. A.* 528 (2010) 273–282. <https://doi.org/10.1016/j.msea.2010.08.079>.
- [40] Y. Zhang, S. Wang, E. Lordan, Y. Wang, Z. Fan, Improve mechanical properties of high pressure die cast Al9Si3Cu alloy via dislocation enhanced precipitation, *J. Alloys Compd.* 785 (2019) 1015–1022. <https://doi.org/10.1016/j.jallcom.2019.01.278>.
- [41] Y. Sui, Q. Wang, B. Ye, L. Zhang, H. Jiang, W. Ding, Effect of solidification sequence on the microstructure and mechanical properties of die-cast Al-11Si-2Cu-Fe alloy, *J. Alloys Compd.* 649 (2015) 679–686. <https://doi.org/10.1016/j.jallcom.2015.07.187>.

- [42] S. Ji, Y. Wang, D. Watson, Z. Fan, Microstructural Evolution and Solidification Behavior of Al-Mg-Si Alloy in High-Pressure Die Casting, *Metall. Mater. Trans. A.* 44 (2013) 3185–3197. <https://doi.org/10.1007/s11661-013-1663-5>.
- [43] Z.-P. Guo, S.-M. Xiong, B.-C. Liu, M. Li, J. Allison, Effect of Process Parameters, Casting Thickness, and Alloys on the Interfacial Heat-Transfer Coefficient in the High-Pressure Die-Casting Process, *Metall. Mater. Trans. A.* 39 (2008) 2896–2905. <https://doi.org/10.1007/s11661-008-9640-0>.
- [44] A.M. Mitrasinovic, F.C. Robles Hernandez, Determination of the growth restriction factor and grain size for aluminum alloys by a quasi-binary equivalent method, *Mater. Sci. Eng. A.* 540 (2012) 63–69. <https://doi.org/10.1016/j.msea.2012.01.072>.
- [45] C.M. Gourlay, A.K. Dahle, Dilatant shear bands in solidifying metals, *Nature.* 445 (2007) 70–73. <https://doi.org/10.1038/nature05426>.
- [46] C.M. Gourlay, H.I. Laukli, A.K. Dahle, Defect band characteristics in Mg-Al and Al-Si high-pressure die castings, *Metall. Mater. Trans. A Phys. Metall. Mater. Sci.* 38 (2007) 1833–1844. <https://doi.org/10.1007/s11661-007-9243-1>.
- [47] BRUCE L. BRAMFITT, The Effect of Carbide and Nitride Additions on the Heterogeneous Nucleation Behavior of Liquid Iron, *Metall. Trans.* 1 (1970) 1987–1995.
- [48] P. Steinmetz, A. Dennstedt, M. Serefoglu, I. Sargin, A. Genau, U. Hecht, Crystal orientation relationships in ternary eutectic Al-Al₂Cu-Ag₂Al, *Acta Mater.* 157 (2018) 96–105. <https://doi.org/10.1016/j.actamat.2018.07.016>.
- [49] S.J. Wang, G. Liu, J. Wang, A. Misra, Characteristic orientation relationships in nanoscale Al-Al₂Cu Eutectic, *Mater. Charact.* 142 (2018) 170–178. <https://doi.org/10.1016/j.matchar.2018.05.037>.
- [50] Q. Lei, B.P. Ramakrishnan, S. Wang, Y. Wang, J. Mazumder, A. Misra, Structural refinement and nanomechanical response of laser remelted Al-Al₂Cu lamellar eutectic, *Mater. Sci. Eng. A.* 706 (2017) 115–125. <https://doi.org/10.1016/j.msea.2017.08.105>.
- [51] I. V. Okulov, S. Pauly, U. Kuhn, P. Gargarella, T. Marr, J. Freudenberger, L. Schultz, J. Scharnweber, C.G. Oertel, W. Skrotzki, J. Eckert, Effect of

microstructure on the mechanical properties of as-cast Ti-Nb-Al-Cu-Ni alloys for biomedical application, *Mater. Sci. Eng. C.* 33 (2013) 4795–4801. <https://doi.org/10.1016/j.msec.2013.07.042>.

- [52] L.M. Kang, C. Yang, F. Wang, X.X. Li, D.Z. Zhu, W.W. Zhang, W.P. Chen, Y. Huan, Designing ultrafine lamellar eutectic structure in bimodal titanium alloys by semi-solid sintering, *J. Alloys Compd.* 702 (2017) 51–59. <https://doi.org/10.1016/j.jallcom.2017.01.257>.